The 22st Annual International Conference on Mechanical Engineering-ISME2014
22-24 April, 2014, Mech. Eng. Dept., Faculty of Eng., Shahid Chamran University, Ahvaz, Iran.

ISME2014-1034

Bubble Rupture under an External Oscillatory Excitation: A Numerical Approach

Ali Omidi[1], Mohammad Passandideh-Fard[2]

[1]Graduate Student, Ferdowsi University of Mashhad; ali.omidi1367@gmail.com
[2]Associated Professor, Ferdowsi University of Mashhad; mpfard@um.ac.ir

Abstract
In this paper, the rupturing of a bubble under an external oscillatory excitation in a cylindrical container is studied using an in-house developed numerical model. The container is occupied by an incompressible liquid. The Volume-Of-Fluid (VOF) method is used to track the liquid-gas interface. The two-step projection method is used to discretize the continuity and momentum equations. The main purpose of this study is the characterization of bubble rupturing phenomenon. The frequency and amplitude effects on the rupturing threshold are evaluated. Furthermore, the effect of the presence and the absence of gravity on this threshold are studied. Finally, a correlation consisting Bond number, Reynolds number and non-dimensional amplitude is provided to capture the bubble-rupturing region. The effect of container walls on the bubble rupturing is also considered. The comparison between the results of numerical simulations and those of the available experiments reveals a good agreement.

Keywords: Bubble rupturing, Normal gravity, Microgravity, Rupturing threshold, VOF method.

Introduction

The understanding of bubble rupturing phenomenon is important in many applications such as acoustic cavitation in turbomachines. The acoustic cavitation is a destructive phenomenon happened in many rotator systems. In this process, the energy of bubbles is suddenly released and the bubble rupturing occurs. In addition, another parameter plays an important role in the rupturing of bubbles. This parameter is the forced oscillations of the bubble.

The bubble rupturing has a significant effect in improvement of the reaction rate, heat transfer and mass transfer in the bubble columns reactors. With due attention to this applications, the identification of bubble rupturing conditions can be desirable for many industrial and physical processes. A cylindrical container including a bubble and water is considered to simulate the process. A sinusoidal motion with different values of frequency and amplitude drives the container. For each amplitude, the frequency of oscillations is increased until the rupturing of bubble occurs. This frequency represents a critical value for the rupturing threshold which is a curved boundary in which the bubble-rupturing occurs.

Yoshikawa et al. [1,2] studied the rupturing of bubble in the normal gravity and microgravity conditions. Their results show that the rupturing threshold in normal gravity is more than that of the microgravity condition. Zoueshtiagh et al. [3] investigated the effects of liquid viscosity, surface tension and size of the bubble on the rupturing phenomenon using experiments. According to these results, the reduction of Bond number and increasing the amplitude increases the rupturing possibility. Shen et al. [4] considered the rupturing of bubble under an acoustic wave excitation. Their results show that using dual frequency excitation decreases the rupturing threshold of the bubble. O'hern et al. [5] experimentally studied the rupturing of a bubble in the silicon oil liquid. Their results show that most of the ruptured bubbles move towards the bottom of the container.

Marmottant et al. [6] provided a new model to investigate the dynamics of bubble covered by a lipid layer. In their study, the rupturing of bubble under ultrasound excitation has been numerically studied. Movassat et al. [7] investigated the role of pressure distribution on the rupturing of a bubble. The effects of the frequency and amplitude on the bubble rupturing were also studied.

The available literature on the rupturing of bubble under forced oscillations is rare and many studies focused on experimental works rather than numerical simulations. Therefore, this study is focused on the rupturing phenomenon of a bubble under forces oscillations and the effects of the important parameters. A correlation is also provided to predict the rupturing region based on dimensionless numbers. The effects of the bubble-wall distance, and the normal and micro gravity conditions are also considered. The simulations are performed using an in-house developed numerical model.

Governing Equations

The fluids are assumed incompressible and Newtonian with a constant viscosity. The conservation of mass and momentum equations are:

$$\vec{\nabla}.\vec{V} = 0 \tag{1}$$

$$\frac{\partial \vec{V}}{\partial t} + \vec{V}.\vec{\nabla}\vec{V} = -\frac{1}{\rho}\vec{\nabla}\mathrm{P} + \frac{1}{\rho}\vec{\nabla}.\left[\mu\left(\vec{\nabla}\vec{V} + \left(\vec{\nabla}\vec{V}\right)^{T}\right)\right] + \frac{1}{\rho}\vec{F}_{ST} - A(2\pi F)^{2} Sin(2\pi F t) \tag{2}$$

where $\vec{V}$ is the velocity vector, ρ the density, μ the dynamic viscosity, P the pressure, and $\vec{F}_{ST}$ represents the surface tension force per unit volume. The last term in the right hand side of the momentum equation specifies the external oscillation force imposed on the

container where A and F indicate the amplitude and frequency, respectively. To track the bubble free surface the following equation is used:

$$\frac{\partial f}{\partial t} + \left(\vec{V}.\vec{\nabla}\right) f = 0 \tag{3}$$

where f represents the liquid volume fraction defined as:

$$f = \begin{cases} = 0 & the\ cell occupied\ by\ air \\ < 1, > 0 & at\ the \text{int} erface\ region \\ = 1 & the\ cell\ occupied\ by\ water \end{cases} \tag{4}$$

To obtain the main dimensionless numbers in the bubble rupturing phenomenon, the momentum equation is non-dimensionalized as:

$$\frac{\partial \vec{V}^*}{\partial t^*} + \vec{V}^*.\vec{\nabla}\vec{V}^* = -\frac{A}{D}\frac{1}{Bo}\vec{\nabla}\mathrm{P}^* + \frac{A}{D}\frac{1}{\mathrm{Re}}\vec{\nabla}.\left[\mu\left(\vec{\nabla}\vec{V}^* + \left(\vec{\nabla}\vec{V}^*\right)^T\right)\right] + \frac{A}{D}\vec{F}_{ST}^* - 4\pi^2\frac{A}{D}Sin(2\pi t^*) \tag{5}$$

where Re and Bo are the Reynolds and Bond numbers, respectively, and D represents the bubble diameter. In this equation, the non-dimensional parameters are defined as:

$$t^* \equiv \frac{t}{T} \equiv tF \tag{6}$$

$$V^* \equiv \frac{\frac{V}{D}}{\frac{}{T}} \equiv \frac{V}{DF} \tag{7}$$

$$\sigma^* \equiv \frac{\sigma}{\rho A D^2 F^2} \tag{8}$$

$$P^* \equiv \frac{\frac{P}{\sigma}}{\frac{}{D}} \equiv \frac{PD}{\sigma} \tag{9}$$

$$\kappa^* \equiv \kappa D \tag{10}$$

$$x^* \equiv \frac{x}{D}, \qquad y^* \equiv \frac{y}{D} \tag{11}$$

In equations (6) to (11), σ is surface tension coefficient, κ the free surface curvature of bubble, x the horizontal axis and y the axis of symmetry. The superscript (*) represents the non-dimensional form of parameters. The important non-dimensional numbers are:

$$\mathrm{Re} = \frac{\rho AFD}{\mu} \tag{12}$$

$$Bo = \frac{\rho A F^2 D^2}{\sigma} \tag{13}$$

$$\frac{A}{D} = non\,\text{dim}ensional\ amplitude \tag{14}$$

Numerical Method

The two-step projection method [8] is used to discretize the continuity and momentum equations. In this method, different terms of the momentum equation are discretized in two fractional steps. First, a temporary velocity is obtained by an explicit discretization of the advective and viscous terms along with surface tension and external oscillatory forces:

$$\frac{\vec{V}^{n+\frac{1}{2}} - \vec{V}^n}{\Delta t} = -\vec{V}^n.\vec{\nabla}\vec{V}^n + \frac{1}{\rho^n}\vec{\nabla}.\vec{\tau}^n + \frac{1}{\rho^n}\vec{F}_{ST}^n - A(2\pi F)^2\sin(2\pi F t^n) \tag{15}$$

Second, the new velocity vector is obtained as:

$$\frac{\vec{V}^{n+1} - \vec{V}^{n+\frac{1}{2}}}{\Delta t} = -\frac{1}{\rho^n}\vec{\nabla}P^{n+1} \tag{16}$$

Taking the divergence of this equation and using the continuity equation leads to the pressure Poisson equation as:

$$\frac{\vec{\nabla}.\vec{V}^{n+\frac{1}{2}}}{\Delta t} = \vec{V}.\left[\frac{1}{\rho^n}\vec{\nabla}P^{n+1}\right] \tag{17}$$

The pressure distribution at the new time level is obtained by solving Equation (17) by means of an Incomplete Cholesky Conjugate Gradient (ICCG) solver [9]. Having obtained the new pressure, the new time level velocities are calculated from Equation (16).

The Youngs PLIC algorithm [10] is used to solve the volume fraction advection equation. The surface tension force term of Equation (2) is modeled using the CSF method [11] as:

$$\vec{F}_{ST} = \sigma\kappa\frac{A_{cell}}{\forall_{cell}}\hat{n} \tag{18}$$

where A_{cell} and $\forall_{cell}$ are cell area occupied by air, and cell volume, respectively. The normal unit vector $(\hat{n})$ is also defined as:

$$\hat{n} = \frac{\vec{\nabla}f}{\left|\vec{\nabla}f\right|} \tag{19}$$

Results and Discussion

The first case considered is that of a 4mm bubble in a cylindrical container under a microgravity condition. The container dimensions and the thermo-physical specifications of fluids are shown in Figure 1 and Table 1, respectively. The result of the simulation for the time evolution of the bubble motion for this case is shown in Figure 2. As observed, dramatic changes in the bubble shape lead to its rupture which can be attributed to a large amplitude (A/D=0.2) and frequency (42 Hz) of the imposed oscillation.

Table 1. The thermo-physical specifications of fluids

Property	Density (kg/m^3)	Dynamic Viscosity $(N.s/m^2)$	Surface Tension (N/m)
Air	1.225	178.94E-7	0.073
Water	998.2	0.001003	

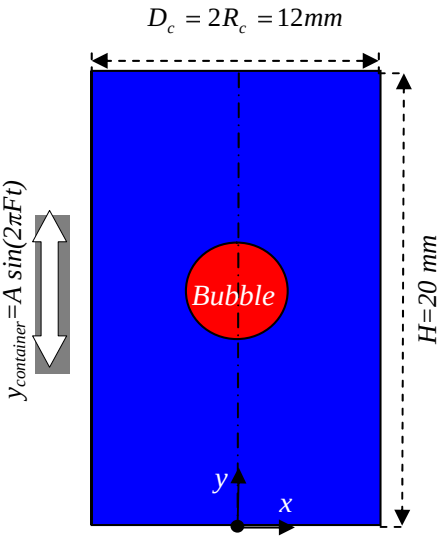

Figure 1. The schematic configuration of a floating bubble in an oscillating container

When the values of the frequency and amplitude are sufficiently high, the bubble breaks up and consequently the smaller pieces of the bubble are suspended in the liquid. For a better understanding of the bubble rupturing phenomenon, the pressure distribution at the rupturing moment (t=22.6ms) is displayed in Figure 3. As the figure shows, a low pressure zone is formed between the two separated smaller bubbles. At this time, a high-pressure gradient around the separation point drives away the surrounding air and replaces water instead; consequently, the bubble-rupturing occurs. This is further explained in Figure 4 where the pressure variations at the rupturing time (22.6 ms) along the axis of symmetry are shown. As seen in the figure, there exit two low pressure points in 12mm<y<13mm range with a high pressure point in between which breaks the air bridge between the two smaller bubbles. The pressure distribution in axial direction varies with time in each bubble oscillating cycle.

Next case considered is that of a 19.69 mm bubble in a 6×6×8 cm container under a microgravity condition, a case for which the experimental results are available in the literature [1]. In this case, at a certain excitation amplitude, the excitation frequency is varied until the bubble rupturing occur. The case is repeated for various values of the excitation amplitude ranged from 0.5 to 11 cm. The frequency of the bubble-rupturing limit, normalized by the natural frequency, is then plotted against the nondimensional amplitude. The comparison between the results of the simulations for these cases with those of the experiment [1] is displayed in Figure 5. The natural frequency of the bubble as introduced by Yoshikawa et al. [1] is defined as:

$$F_n = \left(\frac{4\sigma}{\pi\rho\forall}\right)^{\frac{1}{2}} \qquad (20)$$

where $\forall$ represents the initial volume of the bubble. The small discrepancies observed between the simulations and measurements in Figure 5 may be attributed to the fact that in the numerical simulation, the container was considered a 6cm-dia. cylinder with a height of 8 cm (for a 2D axisymmetric model) while in the experiment, the container had a cubic shape with the same height but with a 6cm-side square base.

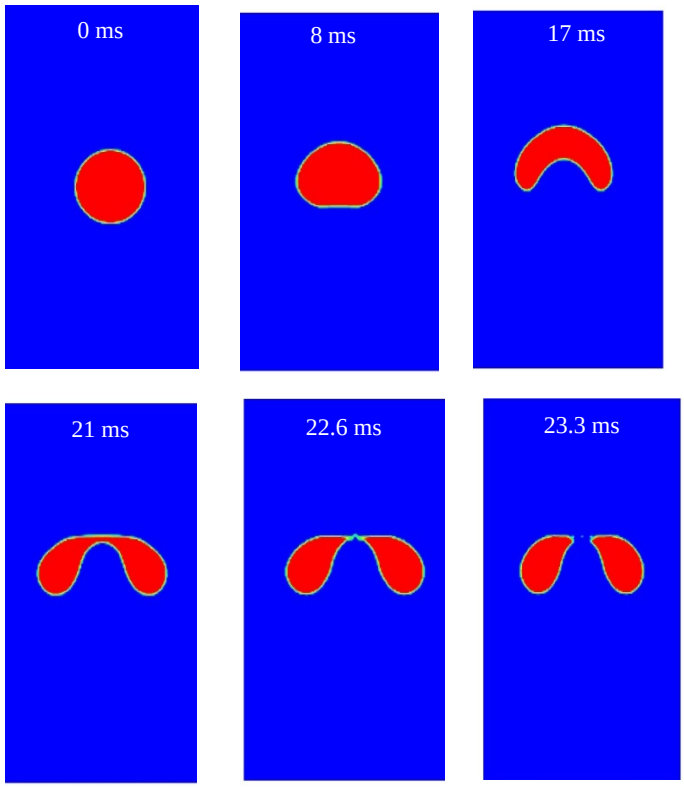

Figure 2. The time evolution of the bubble motion under microgravity condition for A/D=0.2, Bo= 0.3083, Re=133.756

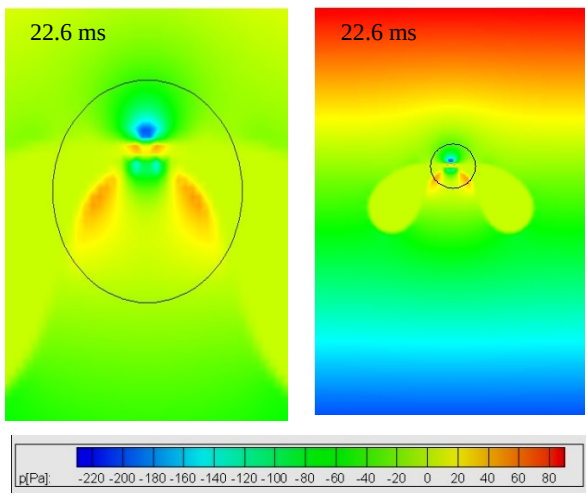

Figure 3. The pressure distribution at t=22.6ms for A/D=0.2, Bo= 0.3083, Re=133.756

The grid independency test of the numerical results is also shown in Figure 5 for two cases: 20 and 30 CPR (Cells per Radius of the bubble). The mean difference between the numerical results corresponding to 20 and 30 CPR is less than 4%. Therefore, a uniform grid with 20 CPR is considered for the rest of simulations in this study.

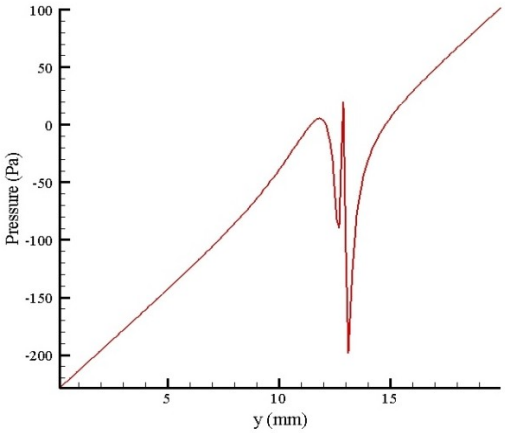

Figure 4. The pressure variations along the axis of symmetry at t=22.6ms

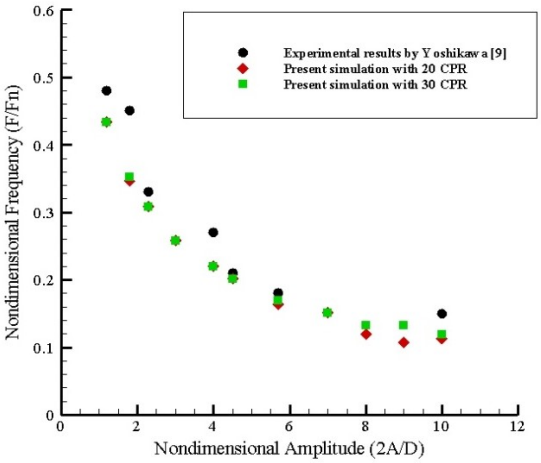

Figure 5. The grid independency and validation of the numerical results

In Figure 6, the critical region of bubble-rupturing under microgravity condition is displayed. The vertical and horizontal axes specify the ratio of Bond to Reynolds number and the non-dimensional amplitude, respectively. As observed, increasing the imposed amplitude decreases the minimum required frequency to break the bubble. While for small amplitudes, the rupturing-limit boundary has a sharp slope, for higher amplitudes the rupturing limit gradually approaches to the horizontal axis. An attempt was made to obtain a correlation for the rupturing limit based on Figure 6. From various curve-fitting attempts, a simple correlation was obtained as:

$$\frac{Bo}{\mathrm{Re}} > 0.0005\left(\frac{A}{D}\right)^{-0.9} \qquad (22)$$

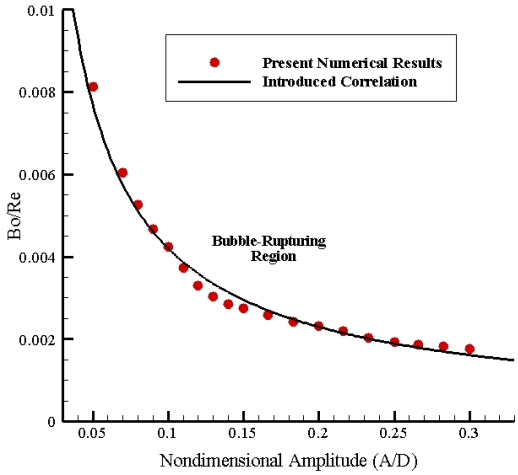

Figure 6. The rupturing threshold of a bubble under microgravity condition

The introduced correlation is plotted in Figure 6. In order to verify the accuracy of the introduced correlation, the predictions from Eq. (22) are compared with a number of measurements and other numerical results available in the literature. This comparison is presented in Figure 7. As seen from the figure, for a wide range of A/D, the introduced correlation accurately predicts the rupturing limit for a bubble under microgravity condition. It is also observed that this correlation results in a more accurate predictions compared to the correlation presented by Yoshikawa [2]. The correlation presented by Yoshikawa et al. [2] is shown in Equation (23).

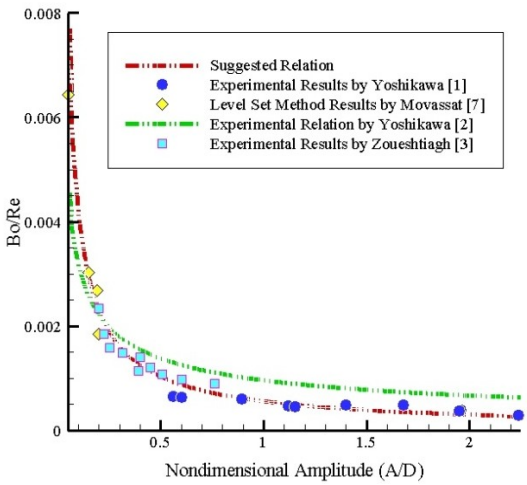

Figure 7. The accuracy of the introduced correlation (Eq. 22) in comparison with other experimental and numerical results

$$\left(\frac{2A}{D}\right)oh^{1.7}\left(\frac{\pi F\rho D^2}{\mu}\right)^{1.92} = 29.3 \qquad (23)$$

where *Oh* represents the Ohnesorge number.

Next, the effects of gravitational acceleration and cylinder walls are investigated. Figure 8 shows the effect of the gravity on the rupturing threshold of a single bubble. The presence of the gravitational force increases the effects of the buoyancy force; consequently, a stronger excitation is required to break

the bubble. In other words, the buoyancy effect postpones the bubble-rupturing phenomenon. For high amplitudes (A/D>0.2), the difference in the rupturing threshold between normal and microgravity conditions is trivial. This may be attributed to that fact that for high amplitudes, the imposed oscillations dominate the effect of the buoyancy force; therefore, the bubble-rupturing easily occurs regardless of the gravitational effects.

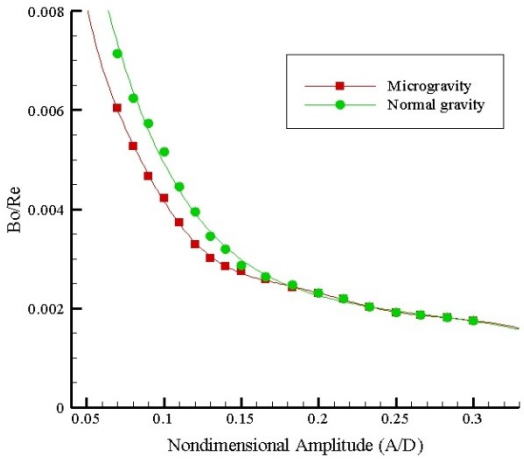

Figure 8. The effect of gravity on the rupturing threshold of a bubble

To investigate the effects of the top and bottom walls on the bubble dynamics during rupturing phenomenon, cylinders with various heights are simulated. Figure 9 shows the effect of the top and the bottom walls on the amplitude response of the bubble. the vertical axis represents the amplitude ratio (the ratio of the bubble to the container amplitude). In this case, the imposed frequency has been considered to be 42 Hz. The effect of the top and bottom walls is minimal when the ratio of container height to initial diameter of the bubble is more than 5.

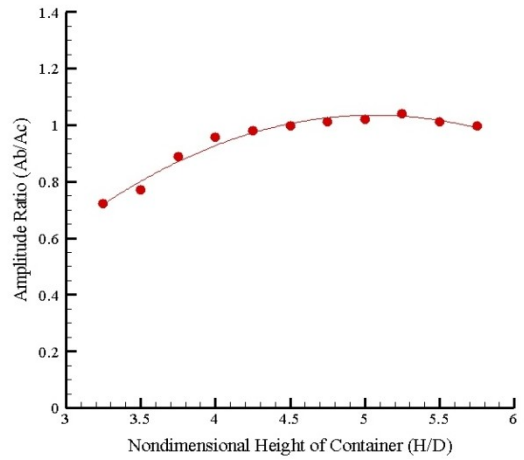

Figure 9. The effect of the top and bottom walls on the bubble amplitude

Conclusions

The rupturing phenomenon of a bubble in a cylindrical container under an external oscillatory excitation was numerically studied. The VOF and two-step projection methods were used in the numerical model. The effects of different parameters such as the Bond number, the Reynolds number, the non-dimensional amplitude, the container walls and the pressure distribution on the bubble-rupturing was investigated. The numerical results compared with those of the experiments. At low amplitudes, increasing the ratio of Bond to Reynolds numbers increases the possibility of bubble-rupturing. From extensive simulations performed this study, a correlation was introduced to capture the critical region of bubble-rupturing phenomenon. The predictions from this correlation were verified with the results obtained from a number of measurements and other numerical results available in the literature. In addition, the bubble response to the external excitation is independent of the container wall effects when the ratio of the container height to the initial diameter of the bubble is more than 5.

List of Symbols

A	Amplitude of oscillations
R_c	Radius of container
D	Bubble diameter
D_c	Diameter of container
H	Height of container
F	Frequency of oscillations
F_n	Natural frequency
f	Volume fraction
$\vec{V}$	Velocity vector
P	Pressure
T	Period of oscillations
t	Time
Re	Reynolds number
Bo	Bond number
Oh	Ohnesorge number
$\hat{n}$	Normal unit vector

Greek Symbols

ρ	Density
μ	Dynamic viscosity
σ	Surface tension
κ	Free surface curvature of bubble

References

[1] Yoshikawa, H., Zoueshtiagh, F., Caps, H., Kurowski, P., and Petitjeans, P., 2007. “Bubble Rupture in a Vibrated Liquid under Microgravity”. *Second International Topical Team Workshop on Two-Phase Systems For Ground and Space Applications*, Tokyo, Japan.

[2] Yoshikawa, H., Zoueshtiagh, F., Caps, H., Kurowski, P., and Petitjeans, P., 2010. “Bubble Spilitting in Oscillatory Flows on Ground and in Reduced Gravity”. *The European Physical Journal E*, Vol. 31, pp. 191-199.

[3] Zoueshtiagh, F., Caps, H., Legendre, M., Vandewlle, N., Petitjeans, P., and Kurowski, P., 2006. “Air Bubbles Under Vertical Vibrations”. *The European Physical Journal E*, Vol. 20, pp. 317-325.

[4] Shen, Ch. Ch., Su, Sh. Y., Cheng, Ch. H., and Yeh, Ch., 2010, "Dual-High-Frequency Ultrasound

Excitation on Microbubble Destruction Volume**",** *Ultrasonics*, Vol. 50, pp. 698-703.

[5] Ohern, T. J., Shelden, B., and Torczynski, J. R., 2011, "Bubble Oscillations and Motion Under Vibration**",** *Physics of Fluids*, Vol. 24, pp. 91-108.

[6] Marmottant, Ph., Van der Meer, S., Emmer, M., Versluis, M., De Jong, N., Hilgenfeldt, S., and Lohse, D., 2005, "A Model for Large Amplitude Oscillations of Coated Bubbles Accounting for Buckling and Rupture**",** *Acoustical Society of America*, Vol. 118, pp. 3499-3505.

[7] Movassat, M., Ashgriz, N., and Bussmann, M., 2012. "Chaotic Shape and Translational Dynamics of 2D Incompressible Bubbles under Forced Vibration in Microgravity". *Microgravity Science and Technology*, Vol. 24, January, pp. 39-51.

[8] Bussmann, M., 2000. "A Three-Dimensional Model of an Impacting Droplet"., Ph.D Dissertation, Toronto.

[9] Kershaw, D. S., 1978. "The Incomplete Cholesky Conjugate Gradient Method For The Iterative Solution of Systems of Linear Equations". *Computational Physics*, Vol. 26, pp. 43-65.

[10] Youngs, D. L., 1984. "An Interface Tracking Method for a 3D Eulerian Hydrodynamics Code". Technical Report 44/92/35, AWARE.

[11] Brackbill, J. U., Cothe, D. B. and Zemach, C., 1992. "A Continuum Method for Modeling Surface Tension". *Computational Physics*, Vol. 100, pp. 335-354.